Int. J. Microgravity Sci. Appl., 33 (3) (2016) 330306
DOI: 10.15011/jasma.33.330306

IIIII ISPS-6 Proceedings IIIII
(Original Paper)

# Formaldehyde LIF-Diagnostics of the Autoignition of n-Decane Droplet Pairs in Microgravity

Christian EIGENBROD[1], Konstantin KLINKOV[1], Michael PETERS[1], Guenther MARKS[1], Wolfgang PAA[2], Volker WAGNER[2] and Wolfgang TRIEBEL[2]

**Abstract**

The interaction between two neighboring n-decane droplets during the autoignition process in air was experimentally investigated under microgravity conditions in the drop tower Bremen. The initial droplet diameter was 0.8 mm in all experiments. Single droplets and droplet pairs with a center distance of 1, 2, 4 and 6 mm were investigated. The air temperature was varied between 650 and 850 K with an increment of 25 K. The examined pressure conditions were 0.3 and 0.5 MPa. This results in a total number of 90 drop experiments. The ignition process was observed applying the laser induced fluorescence (LIF) on formaldehyde with high temporal and spatial resolution. Both, the cool flame process and the hot flame ignition could be measured regarding induction times and the temporal and spatial evolution of the formaldehyde formation.

**Keyword(s):** Droplet ignition, Two stage ignition; Laser-diagnostics
Received 21 October 2015, accepted 27 June 2016, published 31 July 2016.

## 1. Introduction

Knowledge about the physical and chemical processes during autoignition of droplets and sprays at elevated pressure and temperature is essential when aiming for improved combustion systems with lowest emission of pollutants. Pollutant emissions depend to a large extent on the compositions of the air/fuel mixture at the moment of ignition. Important are not only the overall mixture ratio but, in the case of a non- or only partially prevaporized two-phase system, also the local parameters which determine the local flame temperatures and thus e.g. the formation of nitric oxides through the Zeldovich mechanism. Thus, the degree of prevaporization and premixing are important aspects. As mixture formation in a technical system happens in high temperature air at elevated pressure, the mixture formation ends with the autoignition of the ensemble. It is important to note, that a non- or only partially pre-vaporized spray system has shorter induction times compared to a single phased well stirred premixture of the same overall mixture ratio[1,2)]. N-decane in particular is an important model fuel to substitute fossil kerosene in numerical simulations of droplet and spray ignition. It was found that n-decane almost perfectly matches the ignition behavior of synthetic kerosene derived from coal, natural gas or biomass through the Fischer-Tropsch synthesis[3)].

A single droplet in microgravity is the most basic element of a spray. Understanding the physical and chemical processes of single droplet ignition is therefore essential and a prerequisite when aiming for the understanding of more complex systems like multidroplet or spray ignition, convective conditions, non-spherical droplet effects or Marangoni convection effects. Microgravity is an essential tool when performing experiments to validate numerical simulations. For a single droplet, the dimensionality can be reduced to only the radius in numerical simulations, since without natural convection the system is one-dimensional and the transport of matter is only subjected to diffusion and the radial Stefan-flow, which is induced by the difference in volume between the liquid and the gas phase. Therefore, a number of studies have been carried out on single n-decane droplet ignition in microgravity experimentally[3-10)] and numerically[11-31)]. Whereas the number of modeling approaches, mostly including low and high temperature chemical kinetics – some of them are purely analytical – is rather large, the number of experiments for validating purposes is rather low. All these experiments on n-decane droplets applied the droplet suspending and rapid transition technique as used in this study. The suspenders were from quartz, sapphire or silicon carbide with a difference in size, durability at high temperature and in thermal conductivity.

The Michelson interferometry was applied in most of these experimental studies to determine the induction times of cool flame ignition ($\tau_1$) and of hot ignition ($\tau_{tot}$)[7,32)]. This line-of-sight technique is very sensitive to changes of the refractive index which are mainly based on a temperature rise due to the exothermal reactions, but can also be affected by varying

1 ZARM, University of Bremen, Am Fallturm, D-28359 Bremen, Germany
2 Institute of Photonic Technology, Albert Einstein Str. 9, D-07745 Jena, Germany
(E-mail: christian.eigenbrod@zarm.uni-bremen.de)

 

chemical composition. However, it is difficult to detect the beginning of the cool flame when these reactions start smoothly without a strong rise in temperature and thus with only a small gradient of the refraction index. This might be the reason why for some conditions no cool flame was detected[7].

Formaldehyde LIF diagnostics have been applied already in 1998 to fuel drenched porous ceramic spheres[33] and to single igniting n-heptane droplets in 1999[34]. In these drop tower experiments a XeF-excimer laser (353 nm) was used for excitation of formaldehyde. The laser beam was guided into the falling capsule from a laser position between 5 and 120 m apart from the experiment. The research could benefit from these measurements, but the pointing accuracy of the light sheet relative to the falling droplet experiment was too low for extensive parametric studies. The integration of a disk laser into the drop capsule solved this problem[34].

Single droplet experiments cannot reflect on droplet-droplet interactions that play an additional and important role in spray ignition. Experiments on the ignition of droplet pairs in microgravity, focusing on two stage ignition, have not been performed so far. Simulations on droplet-droplet interactions during ignition therefore lack on experimental validation.

## 2. Experimental Setup

### 2.1. Combustion Chamber and Droplet Processing

**Figure 1** shows the experimental setup installed inside the drop vehicle of the Bremen drop tower. The experiments were performed in a pressurized vessel. The upper section contains a resistance heated furnace that is thermally insulated. The furnace has four windows for optical access, three of which were used for these experiments. The lower and cold section of the vessel contains the droplet generation mechanism, the droplet suspender rig and a step motor and belt driven lifting mechanism.

One second after release of the drop capsule, which is the waiting time for thermal convection to relax, the suspender rig is rapidly lifted into the furnace through a narrow opening in the lower insulation. The suspender rig´s motion is optimized regarding acceleration and deceleration in order to be as quick as

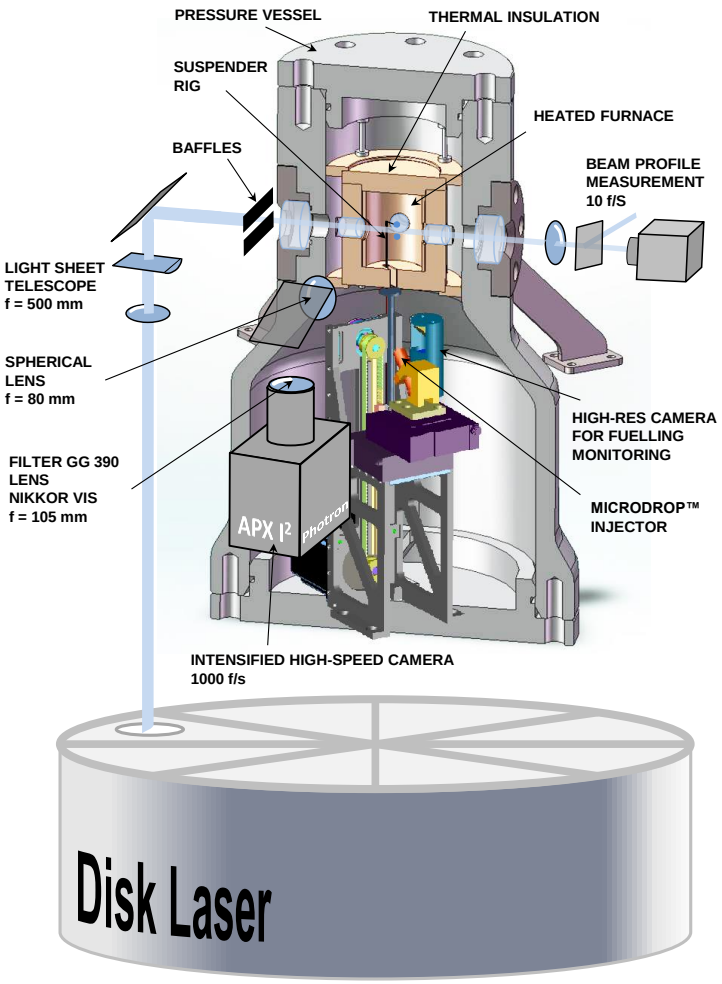


**Fig. 1** Schematics of the experimental setup showing droplet preparation unit, heated furnace and detection system above the laser system.

possible without losing the droplets. The total transition time for the 90 mm distance is 180 ms. The beginning of the induction time ($\tau = 0$) is defined as the moment when the upper droplet enters the insulation and is firstly subjected to heating. From there to the final position the travel distance is 40 mm and the transition time is 50 ms. This was identical for all experiments.

Before releasing the capsule, the droplets were generated in the lower section by injecting a large number of micron sized droplets to the suspenders by means of a piezo driven droplet generator.

The droplet generation was observed and recorded by a high resolution camera with 3840 x 2748 pixels. A single droplet was imaged on 350 pixels. **Figure 2** shows two typical droplets. The short semi-axis amounts initially to 0.72 mm with an accuracy of ± 0.01 mm. This represents a sphere of 0.8 mm in diameter. When exposed to microgravity and heat, the latter leading to a decrease of surface tension, the droplets achieve spherical shape. The suspenders are sapphire rods of 0.15 mm diameter with a molded tip of 0.3 mm diameter. The suspenders are glued horizontally to a vertical thin steel bar which is mounted to the lifting device.

### 2.2 Laser Diagnostic Equipment

Excitation of formaldehyde was achieved in the $\tilde{A}^1A_2 \leftarrow \tilde{X}^1A_1$ system at 343.248 nm. Appropriate excitation light is provided via the third harmonic of a narrowband tunable Yb:YAG disk laser system. The laser system consists of a diode pumped tunable Yb:YAG disk laser c.w. oscillator. It's emission is converted to short pulses of 15 ns duration, which are then seeded into a second Yb:YAG disk laser serving as a power amplifier. The selected wavelength (bandwidth $\Delta\lambda < 1$ pm) is measured by a HighFinesse wavemeter. The amplified pulses are frequency tripled to the near UV spectral region through nonlinear crystals. The energy of the laser was set to 5 mJ at a laser repetition rate of 1 kHz. This enables to record images with a temporal separation of 1 ms, which is fully sufficient for the precise recording of ignition times.

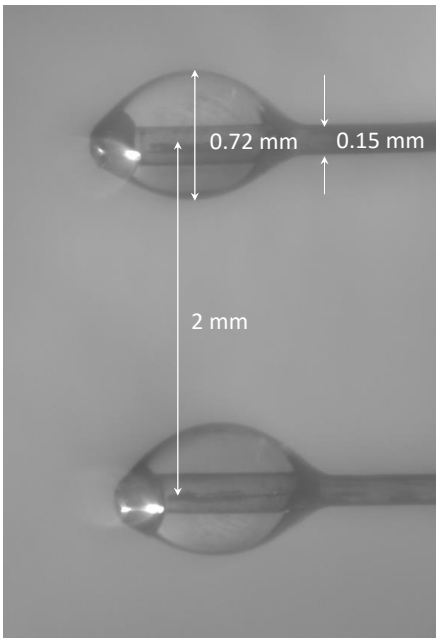


**Fig. 2** Image of suspended droplets of 0.72 mm (short semi-axis) representing spherical droplets of 0.8 mm in diameter. Center distance of suspenders = 2 mm. The image was taken right before release of the drop capsule. When exposed to microgravity and heat, the droplets achieve spherical shape as can be seen in **Figs. 6-10**.

The laser beam is formed to a light sheet of 10 mm in height and a thickness of 0.1 mm by means of a telescope. Precisely adjusted apertures are located in front of the entrance window and protect the droplets from direct laser irradiation.

The energy in the light sheet at the plane of the droplets is attenuated by a dielectric filter behind the outlet window of the vessel and the energy distribution is recorded through an imaging system (CMOS camera of 1600 x 1200 pixel, 10 Hz). These images will be used later to normalize the LIF images.

The LIF signal is taken with a PHOTRON Ultima APX I2 digital video camera on its CMOS sensor of 1024 x 1024 pixels. This intensified camera is operated with 1000 frames/s. A Nikkor VIS lens (f = 105 mm) in combination with a SCHOTT GG 390 longpass filter and an additional lens of f = 80 mm was used. The laser and detection systems are synchronized by a Stanford Research Instruments delay generator. More details of the laser system that was dropped together with the experiment can be found elsewhere[35].

### 2.3 Method of Image Evaluation

In order to extract the data from the videos and to make it accessible for comparison, the pixel intensities were first normalized with the excitation energy profile derived from the light sheet´s energy distribution measurement. Since the variation of the averaged output energy of the laser during one drop experiment is negligible, the time averaged profile was used to normalize the excitation energy distribution. However, the averaged output energy of the laser altered from drop to drop and thus all videos were normalized to the same excitation energy level.

As a next step, an evaluation window was defined covering the droplet´s interspace area and the relative intensity inside this window was calculated and recorded for each LIF image. The total LIF signal inside of this window was defined as unity. The intensity value of the window at the beginning of the recording was defined as zero. **Figure 3** shows how the results of all these normalized values of the ignition process over time are presented as a color coded bar graph for a better contrast.

Since the images were obtained by applying the LIF on formaldehyde with a high-intensified camera, both the cool

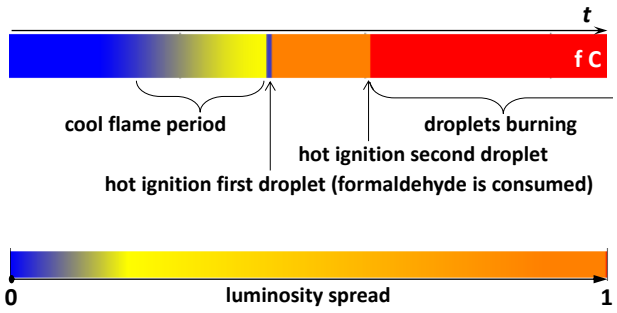


**Fig. 3** Color coded graph displaying the ignition process of a droplet pair.

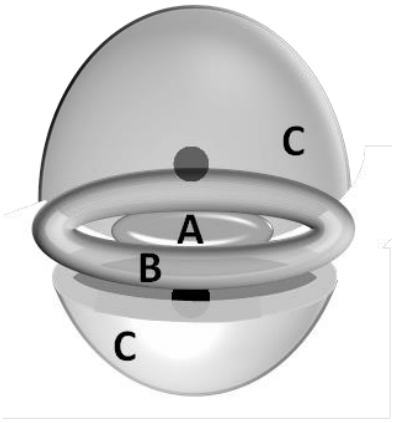


**Fig. 4** Denotation of the location of hot ignition.

flame process and the hot flame ignition could be observed. At the beginning of the recording the region of interest is not visible because formaldehyde is absent (blue color in the diagram). As the cool flame develops, the light intensity rises (yellow color).

During hot ignition, the formaldehyde molecules are immediately decomposed. This is represented by a short dip of intensity. The hot flame is characterized through broadband light emission and Mie scattering of the soot particles. Thereby, the hot flame region of the image is bright and the color diagram becomes either orange (one droplet burns) or saturated red (two droplets burn).

The character f in the bar graph describes the spatial and temporal process of formation of the cool flame. Three types of cool flame ignition could be distinguished: 1. with a clear and sharply identifiable front **(f)**, 2. with some front but rather diffuse **(df)**, or 3. slowly growing and diffuse **(d)** buildup without a well-determined location.

The character **C** printed into the bar graph delivers additional information on the location of the hot ignition. **Figure 4** shows how the different locations are denoted. For reasons discussed in **Chap. 3** the hot ignition may happen in three different areas which is either in between the droplets **(A)** or outward of the interspace **(B)** or towards the outside of the droplets **(C)**. In the case that two droplets ignited independently it is indicated as **(2)**.

## 3. Results and Discussion

In order to give a clear picture of the observed processes and to allow an easy comparison, the results of all experiments are summarized in **Fig. 5** in a way as explained in **Figs. 3 and 4**. As hot flame burning time is not an issue here, the duration of hot burning is truncated after 100 ms to enhance the depiction of the period of the ignition process.

In general there exist three prerequisites for hot flame ignition: 1. It needs the appropriate mixture of fuel and air; 2. It needs the right temperature to produce enough formaldehyde and OH-radicals[3)]; 3. It requires enough time for the right mixture at the appropriate temperature to initiate thermal runaway. It is assumed that even when the concentration of radicals is maximal at the droplet´s interspace decreasing towards the outbound, the temperature there can be too low due to the phase change enthalpy which is consumed by the two droplets. Therefore, ignition happens at a position where concentration and temperature provide the best conditions which also may be at the boundary of the droplet´s interspace.

The following inverted raw images show characteristic cases of ignition. **Figure 6** shows a situation at 650 K with a steep rise of the formaldehyde formation rate at the beginning (650 ms). In this case it might be meaningful to define it as the induction time to cool flame burning. The hot ignition indicated by a hole burnt into the formaldehyde cloud happens firstly at the boundary of the droplet´s interspace after 818 ms (arrow in **Fig. 6**).

**Figure 7** shows images of the same configuration but at 750 K. In this case, the definition of a first induction time was difficult because the formaldehyde formation happened without clear space-time front. The hot ignition appeared at almost the same location (after 413 ms, arrow), but the spreading of the hot flame was rather slow before it engulfs both droplets.

When the distance of the droplets rises to 4 mm, the situation changes. **Figure 8** shows that now the distance is large enough that the best location for hot ignition apparently moves towards in between the droplets (497 ms). Increasing the pressure from 0.3 to 0.5 MPa has the same effect as increasing the droplet´s distance. **Figure 9** shows this situation with the same conditions as before but at 0.5 MPa instead of 0.3 MPa. Now, the upper droplet ignites first after 392 ms. The hot ignition now happens at the upper right and is thus not anymore related to the droplet´s interspace.

This seems to be reasonable as we can see that the formaldehyde LIF intensity already decreases between the droplets. There, the formaldehyde LIF intensity is still high, but the temperature must be lower than at the outbound sides due to

the two droplets´ cooling effect. When the droplet´s interspace is no longer decisive, it is arbitrary whether the upper or lower droplet ignites first and where it happens circumferentially.

The most independent ignition of droplets appeared in experiments with a droplet distance of 6 mm and at a pressure of 0.5 MPa. In these cases cool and hot ignitions can be observed almost individually in space as well as in time.

Thus, the induction times for cool and hot flame ignition are

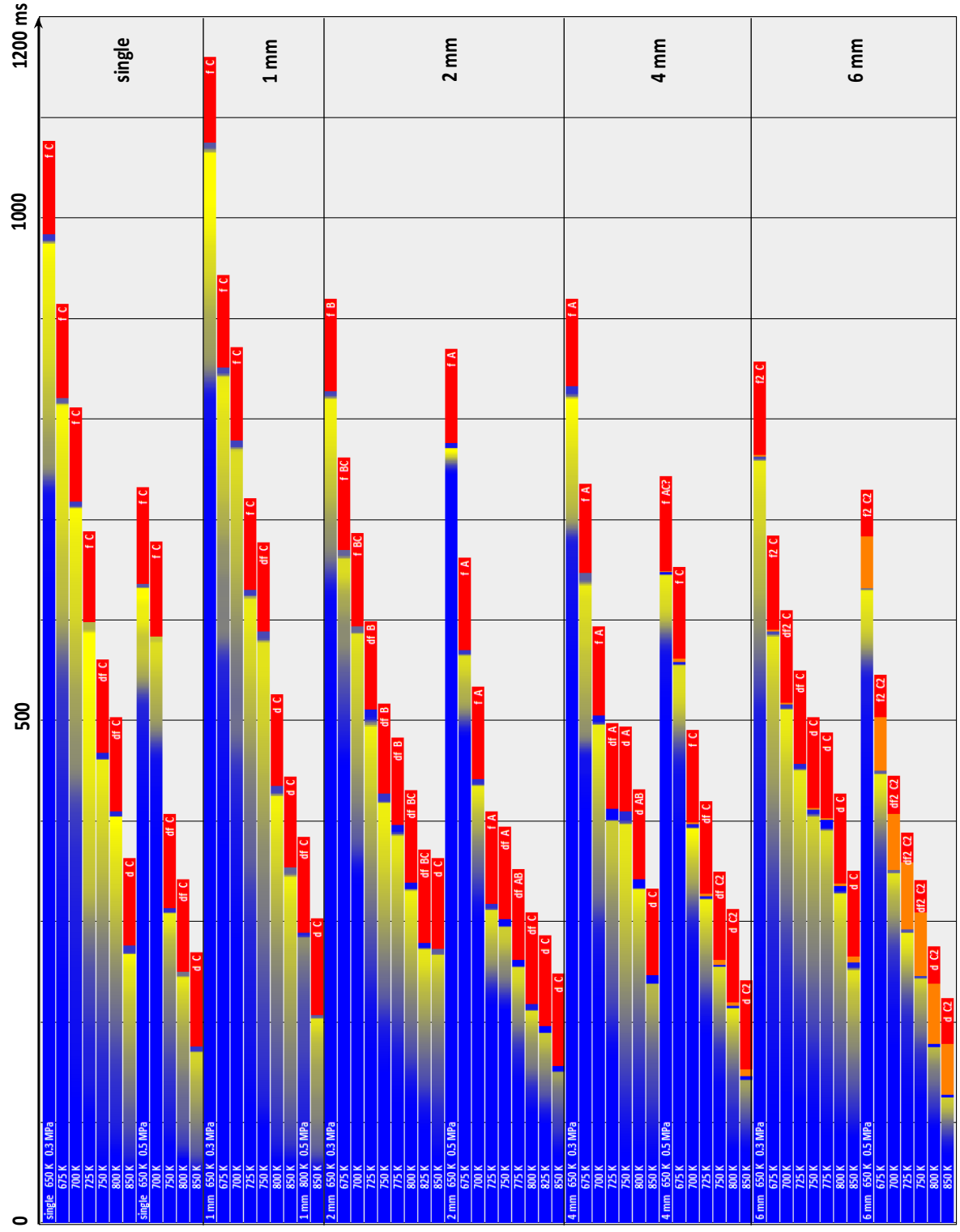


**Fig. 5** Summary of experimental results. Notations describe distance between droplets, initial pressure, ambient temperature and location and type of cool flame ignition.

expected to approach those of a single droplet. However, the induction times are the shortest of all experiments with the largest difference to a single droplet (- 20 % in average). This can only mean that droplets at a 6 mm distance are not individual at all and free from interferences between each other. Whereas it is clear that from a certain distance on droplet pairs will ignite like single droplets, which distance beyond 6 mm remains open.

Since the induction times drop more or less monotonically with rising droplet´s distance, the results appear plausible. In order to assure the plausibility of the single droplet data, the experiments were not only repeated, but they were also tested with a two droplet rig with only the lower or the upper suspender rig being fueled. Even though the lower droplet position shows slightly longer induction times, the spread between results for identical parameters times, the spread between results for identical parameters was never larger than 10 %. So it must be asserted that the ignition of droplet pairs

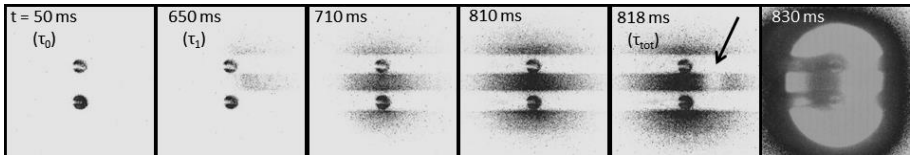


**Fig. 6** Selected images of an experiment at 650 K, 0.3 MPa and 2 mm droplet distance. Through image 2 to 4 the development of the cool flame is clearly visible. At $\tau$ = 818 ms the hot ignition firstly burns a hole into the formaldehyde cloud (arrow). All images are normalized concerning the excitation energy.

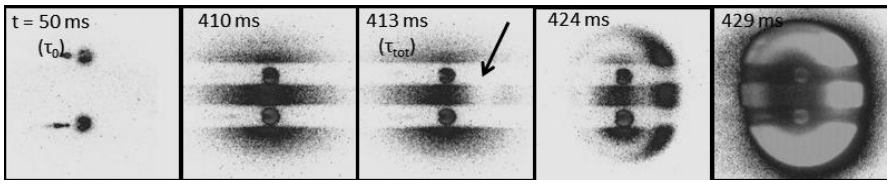


**Fig. 7** Selected images of an experiment at 750 K, 0.3 MPa and 2 mm droplet distance. The arrow indicates the location and first appearance of hot ignition again detected through a region where formaldehyde is consumed.

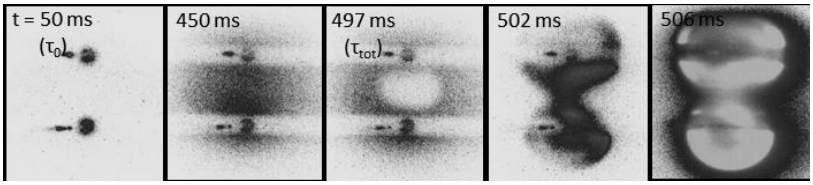


**Fig. 8** Selected images of an experiment at 700 K, 0.3 MPa and 4 mm droplet distance. At $\tau$ = 497 ms hot ignition is initiated in between the droplets.

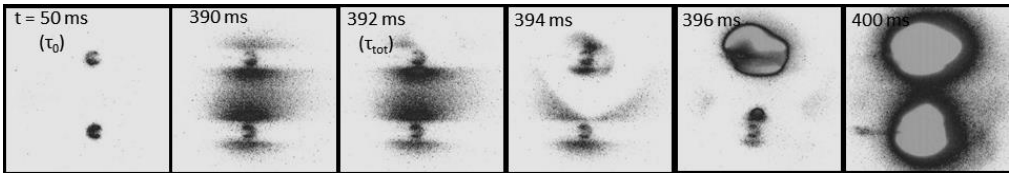


**Fig. 9** Selected images of an experiment at 700 K, 0.5 MPa and 4 mm droplet distance. At $\tau$ = 392 ms hot ignition happens at the upper right of the upper droplet.

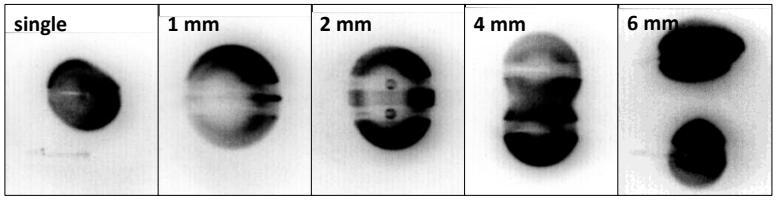


**Fig. 10** Hot flame ignition of experiments at 750 K, 0.3 MPa with a single droplet and pairs of droplets at different distances.

confirms the complexity of the interplay between the three prerequisites stated at the beginning of this section. Whether local temperature or local mixture ratio or residence time determine ignition can now be clarified through numerical simulations. It should be noted here that the overall air/fuel ratio theoretically established in the furnace after complete vaporization of a single droplet and after well stirred mixing is approx. 50 or 25 for two droplets respectively.

As can be seen in **Fig. 5**, the cool flame ignition has a clear front (**f**) in experiments with lower initial ambient temperature. The cool flame ignition was initiated in outside regions (**C** or **B**, see **Fig. 4**) and moved straight through a droplet´s location to the opposite side. As information can only be gathered from inside the light-sheet it is assumed that at lower temperatures the cool flame builds up first in the more distant regions and then propagates towards the droplet(s). The velocity of the flame front propagation can be evaluated as 0.05-0.1 m/s. With rising ambient temperature the ignition front of the cool flame becomes more diffuse (**df**). That indicates, that the buildup region is less localized and distributed over a larger volume. We know that the induction to cool flame ignition is temperature and not concentration dependent [1)]. But it´s detectability through LIF of course depends on concentrations. When the initial formation of formaldehyde is too small to be detected and happens far from the droplets in a region of low fuel concentration and higher temperature, then it is detected when the temperature and thus the formation rate has already increased in the light-sheet. These overlaying effects might be the reason for the diffuse appearance. At high ambient temperature the induction to cool flame is always detected to happen everywhere with no front and a more or less homogeneous buildup.

In contrast to the cool flame ignition, the hot flame ignition was always initiated in the droplet´s near-field and spread around the droplet/droplets within 4-6 ms. The diameter of the hot domain changed with pressure and ambient temperature: from 5 mm at 0.3 MPa/ 650 K to 2 mm at 0.5 MPa/ 850 K in experiments with single droplets. For specific configurations (0.3 MPa/ 0.5 MPa with 1 mm droplet´s distance, and 0.3 MPa with 2 mm droplet´s distance) the single hot domain was observed to be shared by both droplets (see **Fig. 10**). In other cases with pairs of droplets the individual hot spheres could be clearly determined.

It should be noted that at high temperature, high pressure and larger droplet distances the cool flame burning can be very short and cool and hot flame ignition are separated by only < 50 ms. However, hot flame ignition without a preexisting cool flame was in no case detected.

Collected experimental data cover a wide range of patterns of the cool flame evolution as well as the hot ignition of droplet pairs. The results contain valuable information for developing numerical simulations that consider the ignition and combustion phenomena in a heterogeneous air-fuel mixture.

## 4. Conclusion

Experiments on the autoignition of pairs of n-decane of different droplet distance in a hot pressurized ambience showed, that the induction times to cool- and hot flame ignition are not only temperature and pressure dependent but do also depend on the droplets distance. A droplet pair of 1 mm droplet distance has a slightly longer induction time than single droplets at all investigated temperatures and pressures. This is assumed to be attributed to the cooling effects through vaporization that seem to supersede the effect of exposing more fuel/ volume. With increasing droplet distance the situation changes. The wider the distance, the shorter the induction times become. In these cases the fuel/ volume increase seems to supersede the cooling effect. Even with 6 mm droplet distance, when the droplets ignited individually at all investigated parameters, the droplet pair does still not behave like two single droplets. In contrast, this situation exhibited the shortest induction times. In contrast to former publications on single droplet ignition, it could not be validated, that the induction time to cool flame burning is temperature dependent while the cool flame burning time is pressure dependent. In contrast, for the droplet pairs both values depend on temperature and pressure. The relatively shortest cool flame burning times appeared at 2 mm/ 0.5 MPa.

It was found that for the closest (1 mm) and the widest (6 mm) droplet distance, hot ignition happens only somewhere outbound the droplet pair while for intermediate droplet distances the location of hot ignition was in between the droplets or outbound the symmetry plane. The latter was predominantly only the case for 2 mm/ 0.3 MPa. In conclusion it can be summarized, that hot ignition happens outside the droplet pair for wide distances moving towards in between for intermediate distances and is “squeezed out” the interspace when droplets get even closer.

## Acknowledgements

This work has been supported by the German Space Management (DLR) Office for Research under Space Conditions under Grant No. 50WM1125 within the project: “Droplet-Droplet Interactions” which is gratefully acknowledged.

## References

1) O. Moriue, M. Mikami, N. Kojima and C. Eigenbrod: Proc. of the Combustion Institute (2004).
2) Z. Bouali, C. Pera and J Réveillon: European Combustion Meeting (2009).
3) C. Eigenbrod, F. Giese, M. Reimert, P. Rickmers and K. Klinkov: IGTI Turbo-Expo, Power for Land, Sea and Air, ASME (2013).
4) M. Reimert: Doctoral Thesis, University of Bremen, Germany (2012).

5) T. Bolik, J. König, C. Eigenbrod and H.J. Rath: Microgravity, Sci. Tech., **13** (2001) 1.
6) O. Moriue, C. Eigenbrod, H.J. Rath, J. Sato, M. Tsue and M. Kono: Space Forum, **6** (2000) 1.
7) O. Moriue, C. Eigenbrod, H.J. Rath, J. Sato, K. Okai, M. Tsue and M. Kono: Proc. of the Combustion Institute (2000).
8) T. Bolik, J. König, C. Eigenbrod and H.J. Rath: 10th International Symposium on Applications of Laser Techniques to Fluid Mechanics (2000).
9) C. Eigenbrod, O. Moriue, P. Weilmünster and H.J. Rath: Fraunhofer-Inst., für Chem., Tech., (28th International Annual Conference) (1997).
10) J. König, C. Eigenbrod, M. Tanabe, H. Renken and H.J. Rath: 26th Symposium (Int.) on Combustion (1996).
11) V.B. Betelin, N.N. Smirnov, V.F. Nikitin, V.R. Dushin, A.G. Kushnirenko and V.A. Nerchenko: Acta Astronautica, **70** (2012).
12) I. Dhuchakallaya and A.P. Watkins: Applied Energy, **87** (2010).
13) O. Herbinet, W.J. Pitz, and C.K. Westbrook: Combustion and Flame, **157** (2010).
14) S.M. Frolov, V.Ya. Basevich, F.S. Frolov, A.A. Borisov, V.A. Smetanjuk, K.A: Avdeev, A.N. Gots: Russian J. of Phys. Chemistry, **B(3)** (2009).
15) I. Dhuchakallaya, A.P. Watkins: Applied Mathematical Modelling, **34** (2010).
16) S.S. Sazhin: Progress in Energy and Combustion Science, **32** (2006).
17) S.S. Sazhin, T. Kristyadi, A. Abdelghaffar and M.R. Heikal: Fuel, **85** (2006).
18) F. Buda, P.A. Glaude, F. Battin-Leclerc, R. Porter, K.J. Hughes and J.F. Griffiths: Journal of Loss Prevention in the Process Industries, **19** (2006).
19) S.S. Sazhin, W.A. Abdelghaffar, E.M. Sazhina and M.R. Heikal: International Journal of Thermal Sciences, **44** (2005).
20) A. Cuoci, M. Mehl, G. Buzzi-Ferraris, T. Faravelli, D. Manca and E. Ranzi: Combustion and Flame, **143** (2005).
21) M. Costa, B.M. Vaglieco and F.E. Corcione: Experiments in Fluids, **39** (2005) 3.
22) J.F. Griffiths, K.J. Hughes and R. Porter: Proc. of the Combustion Institute (2004).
23) O. Colin, A.P. da Cruz and S. Jay: Proc. of the Combustion Institute (2004).
24) J.C. Beck: Proc. Mathematical, Physical and Engineering Sciences, **459** (2003).
25) S. Schnaubelt, O. Moriue, C. Eigenbrod and H.J. Rath: Microgravity, Science and Technology, **XIII(1)** (2001).
26) C.K. Westbrook, H.J. Curran, W.J. Pitz, J.F. Griffiths, C. Mohamed and S.K. Wo: Proc. Combust. Inst., **27** (1998).
27) F.F. Fachini and A.M. Linan: Combustion and Flame, **109** (1997).
28) J.F. Griffiths: Progress in Energy and Combustion Science, **21** (1995).
29) J.F. Griffiths: Combustion and Flame, **93** (1993).
30) W.A. Sirignano: Numerical Simulation of Combustion Phenomena (1985).
31) M.P. Halstead, L.J. Kirsch and C.P. Quinn: Combustion and Flame, **30** (1977).
32) M. Tanabe, M. Kono, J. Sato, J. König, C. Eigenbrod, F. Dinkelacker and H.J. Rath: Combust. Sci. and Tech., **108** (1995).
33) J. König, C. Eigenbrod, T. Bolik, H.J. Rath, D. Grebner, D. Müller and W. Triebel: 27th Symposium (International) on Combustion (1998).
34) J. König, C. Eigenbrod, H.J. Rath, D. Grebner, J. Hein and W. Triebel: 1999, 5th Intl. Microgravity Combustion Workshop, Cleveland (1999).
35) V. Wagner, W. Paa, W. Triebel, C. Eigenbrod, K. Klinkov, M. Larionov, A. Giesen and C. Stolzenburg: Review of Scientific Instruments, **85** (2014).